On analytical approximations for the structure of a shock wave in a fully ionized plasma

D. Domínguez-Vázquez[1] and R. Fernandez-Feria[1]
[1]*Fluid Mechanics, Universidad de Málaga, Dr Ortiz Ramos s/n, 29071 Málaga, Spain*

(Dated: 2 August 2019)

Two approximate solutions for the shock wave structure in a fully ionized plasma are given for weak and moderately strong shocks. Both solutions are algebraically very simple in the phase space of the electron and ion temperatures as functions of the plasma velocity, being algebraically more involved in the physical spatial coordinate, except when constant electron conductivity is assumed. One solution is based on the observation that for weak, relaxation shocks the electron and ion temperatures are very close to each other. However, for sufficiently large ionization (atomic) number Z this solution is valid even for any difference between both temperatures, capturing quite accurately the ion temperature overshoot appearing in moderately strong relaxation shocks for large Z. For stronger shocks with an internal ion shock this first approximate solution remains quite accurate in the preheating region upstream of the inner shock, but not in the relaxation downstream region. For this latter region we find another good algebraic approximation based on the almost constancy of the electron entropy. The combination of these two approximations upstream and downstream of the inner shock, connected through the also algebraic Rankine-Hugoniot relations for the inner shock, provides a good approximation for the entire shock structure even for moderately strong shocks. These algebraic approximate solutions are compared with exact numerical solutions for several values of the Mach and ionization numbers. Some relevant features such as the shock thickness and the ion temperature overshoot are analyzed.

I. INTRODUCTION

The structure of a shock wave in a fully ionized, collisional plasma is a well-studied problem, both at the fundamental level for the wave propagating through a quasineutral fully ionized gas,[1–7] or considering the effect of some additional physical features such as, for example, nonlocal electron heat conduction,[8] the presence of an electric current or field,[9] or gray radiation diffusion.[10,11] The subject continues to be of great physical interest in the study of inertial fusion,[12,13] particularly for the study of the shock ignition of thermonuclear fuel,[14,15] or in the related problem of creating a sharp, controllable plasma density gradient at the interface between vacuum and a gaseous medium using a laser generated shock wave.[16] In simulations codes for these processes the electron heat conduction and the inclusion of plasma models with separate ion and electron temperatures are both very relevant, for which the planar shock wave constitutes a benchmark for validation, particularly when analytical solutions, like those derived in the present work, are available. The subject is also of interest in some astrophysical problems such as the shock waves produced by supernovae and other explosive phenomena in the universe, star formation, accretion flows, the shock generated when the solar wind slams into Earth's magnetic field, among others,[17,18] though in many of these astrophysical plasma shock waves the Mach number is quite large and radiation becomes relevant, which is not considered in the present work.[10,11,18,19] We also do not consider here the case of a shock wave propagating in a weakly ionized plasma,[20–22] of great recent interest in hypersonic aircraft flow control and in plasma assisted combustion.[23,24]

The set of ordinary differential differential equations governing the simplest two-dimensional and stationary plasma shock wave, reviewed in §II below, have to be solved numerically, which is sometimes a very hard task due to the different singular points and length scales, particularly when an inner shock appears inside the wider plasma shock wave structure. For this reason it is always quite useful to have analytical solutions, either approximate or exact in some particular limits, that additionally may help to better understand the physics and the structure of the flow. This is a known practice for the shock wave structure in neutral gases. For instance, Becker[25] found an analytical solution for the shock wave of a neutral gas with constant transport coefficients and a particular value of the Prandtl number, latter improved by Morduchov and Libby,[26] and Johnson,[27] who also obtained closed-form solutions in the limits of large and small Prandtl number.[27,28] Analytical approximate solutions have also been found in the problem of the shock wave in a binary gas mixture with mass disparity, either assuming almost constant light gas entropy,[29] or in the limit of small Prandtl number of the light gas.[30] This problem is somewhat similar to the plasma shock wave, with two velocities, one for each neutral gas species, and just one temperature, instead of the two temperatures (electron and ion temperatures) and only one velocity considered in the present study, where quasineutrality is assumed for the fully ionized plasma. Some semi-analytical solutions exist for this problem of a shock wave in a plasma in the equilibrium diffusion limit with just one temperature,[10,19] or combination of analytical solutions in the phase space for specific regimes with numerical solutions in the physical space,[7] but we have not found analytical approximate solutions in the literature for the complete plasma shock wave, that includes the case of moderately strong shocks with embedded ionic shock, which are given here in both the phase and the physical spaces. In particular, in the present paper we describe two analytical solutions which approximate the flow structure inside a shock wave in a fully ionized plasma, both upstream and downstream, so that an approximate global structure can be constructed which helps to understand the flow physics inside the shock. The analytical approximate expressions are interesting to evaluate relevant physical features of the plasma shock such as the ion tempera-

ture overshoot and the shock wave thickness, both considered in the present paper, and also to verify hydrodynamic codes using plasma physics models, to analyze the hydrodynamic stability of shock fronts in plasmas, etc. The approximate structures of the shock wave for several values of the Mach number and different ionization numbers are discussed and compared with exact numerical solutions of the shock wave differential equations.

II. EQUATIONS, SHOCK WAVE STRUCTURE AND NUMERICAL SOLUTIONS

We consider the structure of a two-dimensional planar shock wave in a fully ionized plasma using the formulation of Jaffrin and Probstein.[4] These authors derived the shock wave equations for ionization number $Z = 1$ (actually, Z is the atomic number for a fully ionized plasma), later generalized by Ramirez et al.[8] for any value of Z. We just give in this section the shock equations with a brief summary of its structure, together with some numerical results.

In the formulation of Jaffrin and Probstein[4] it is assumed that Debye length is much smaller than any collisional mean free path, so that quasineutrality applies and the electromagnetic problem is decoupled from the (thermo-)mechanical one. The problem is thus described by an unique velocity field for the electrons and ions, and two separate temperatures, one for the electrons and another one for the ions. The non-dimensional equations describing the shock wave structure in terms of the velocity $\eta = \eta_e = \eta_i$ (subscript 'e' refers to the electrons and 'i' to the ions), the electron temperature θ_e and the ion temperature θ_i can be written, for any value of Z, as[4,8]

$$\theta_i = \frac{5M_2^2}{3}(Z+1)\eta\left[\left(\frac{3}{5M_2^2}+1\right)-\eta\right]-Z\theta_e, \qquad (1)$$

$$\frac{d\theta_e}{dy} = \frac{4M_2^3}{\theta_e^{5/2}}(\eta-1)(\eta_1-\eta), \qquad (2)$$

$$\frac{d\eta}{dy} = \frac{Z\dfrac{d\theta_e}{dy}+\dfrac{36Z^2}{25(Z+1)^2}\dfrac{k_0(\theta_e-\theta_i)}{M_2\eta^2\theta_e^{3/2}}}{\dfrac{1}{3}(Z+1)\left[\dfrac{5}{3}(5-8\eta)M_2^2+5\right]-\dfrac{2}{3}Z\dfrac{\theta_e}{\eta}}. \qquad (3)$$

Note that the total momentum equation (1) corresponds to Eq. (17) in Ref.[8], the total energy conservation equation (2) to Eq. (A1) in that reference, while the ion energy equation (3) is Eq. (A2) in Ref.[8], but with one of its terms written differently by using Eq. (2) (notice also that there is a misprint in this equation (A2) of Ref.[8], where the term $\gamma_0(Z)/M_2^2$ should be k_0/M_2 in the local electron conductivity limit, with M_2 and k_0 defined below, like any other quantity used in these equations, which also coincide with Eqs. (4.1), (4.7) and (4.8), respectively, in Ref.[4] when $Z = 1$, but with the non-dimensional spatial coordinate defined in a slightly different form).

In these equations, the nondimensional variables are defined as

$$y = \frac{x}{H_I}, \quad \eta = \frac{U}{U_2} = \frac{n_2}{n}, \quad \theta_i = \frac{T_i}{T_2}, \quad \theta_e = \frac{T_e}{T_2}, \qquad (4)$$

where x is the spatial coordinate, scaled with a characteristic length H_I defined below; $U = U_e = U_i$ is the velocity, T_e and T_i are the electron and ion temperatures, respectively, and $n = n_e = n_i Z$ is the electron number density, related to the ion number density n_i through the ionization number Z, and also related to the velocity by mass conservation, $m_e nU =$ constant $= m_e n_2 U_2$, say, where m_e is the electron mass and the subscript '2' refers to the downstream conditions ($x \to \infty$). All the flow magnitudes are scaled with their corresponding downstream values, so that

$$\eta_2 = 1, \quad \theta_{e2} = \theta_{i2} \equiv \theta_2 = 1. \qquad (5)$$

The upstream values ($x \to -\infty$, denoted by the subscript '1') are given by the Rankine-Hugoniot relations resulting from Eqs. (1)-(3) for vanishing gradients:

$$\eta_1 = \frac{M_2^2+3}{4M_2^2} = \frac{4M_1^2}{M_1^2+3}, \qquad (6)$$

$$\theta_1 = \frac{\left(M_2^2+3\right)\left(5M_2^2-1\right)}{16M_2^2} = \frac{16M_1^2}{\left(M_1^2+3\right)\left(5M_1^2-1\right)}, \qquad (7)$$

(8)

with the upstream and downstream Mach numbers defined as

$$M_\alpha^2 = \frac{m_i U_\alpha^2}{\gamma(Z+1)kT_\alpha}, \quad \alpha = 1,2, \qquad (9)$$

and related through

$$M_2^2 = \frac{M_1^2+3}{5M_1^2-1}. \qquad (10)$$

Note that $T_e = T_i = T_\alpha$, at the upstream ($\alpha = 1$) and downstream ($\alpha = 2$) conditions. In (9), k is Boltzmann constant, through which both pressures p_e and p_i are related to their corresponding temperatures, $p_{e,i} = n_{e,i}kT_{e,i}$, and $\gamma(= 5/3)$ is the ion's heat capacity ratio. Mach number M_1 varies from unity to infinity, while M_2 is limited from 1 to $1/\sqrt{5}$.

The length scale H_I used to nondimensionalize equations (1)-(3) is proportional to the mean-free path for ion-ion scattering evaluated at downstream conditions, $l_2 = \sqrt{kT_2/m_i}\,\tau_{i2}$, with $\tau_{i2} = [3m_i^{1/2}(kT_2)^{3/2}]/[4\pi^{1/2}e^4Z^4n_{i2}\ln\Lambda_i]$ the ion-ion collision time at downstream conditions ($-e$ is the electron charge and m_i the ion mass), divided by the square root of the mass ratio,[4,8]

$$H_I = \frac{6\sqrt{3}k_0Z^3\ln\Lambda_i}{5\sqrt{5}(Z+1)^{3/2}\ln\Lambda_e}\,\frac{l_2}{\varepsilon}, \quad \varepsilon = \sqrt{\frac{m_e}{m_i}} \ll 1, \qquad (11)$$

where $k_0 \simeq 3.906$ is a constant appearing in the ionic thermal conductivity $\kappa_i = k_0 n_i k T_i \tau_i / m_i$,[31] and $\ln\Lambda_e$ and $\ln\Lambda_i$ are the electron and ion Coulomb logarithms.[32] Note that under the quasi-neutrality hypothesis, Coulomb logarithms can be

assumed constants, so that viscosity and thermal conductivity are proportional to $T^{5/2}$ for both ions and electrons.

As explained by Jaffrin and Probstein,[4] since H_I is much larger than the ion-ion mean free path, ion viscous terms (and, of course, electron viscous terms, which are ε times smaller) have been neglected in the total momentum conservation equation (1), in the total energy conservation equation (2), and in the ion energy conservation equation (3). Likewise, the ion heat conduction terms have been neglected in Eqs. (2) and (3). Finally, it is worth mentioning here that the energy transfer between ions and electrons have been assumed linear with the temperature difference in Eq. (3).[31]

Equations (1)-(3) model the so called *external problem*, with length scale H_I, where only two dissipative mechanisms are present at the lowest order in ε: electronic heat flux and energy transfer between electrons and ions.[1,3–6,8] However, as first described by Imshennik,[3] above a critical Mach number M^*, which will be given below, there exists a much thinner *inner, or ionic, shock* where ion viscous terms are relevant. The thickness of this inner shock is of the order of the ion-ion mean free path, $H_{II} \sim l_2$, so that ion viscous terms are relevant, but the electron temperature remains almost constant (at the lowest order in ε) inside this inner region. Thus, for $M > M^*$, the structure of the shock consists of (see, for instance, Fig. 2 below for an example) a preheating external region I of thickness of order H_I and governed by (1)-(3), a inner region II of much smaller thickness H_{II} where the electron temperature remains constant while the velocity decreases and the ion temperature increases, and a relaxation zone III, also of thickness of order H_I and governed by (1)-(3), where the temperatures and velocity evolve towards their final equilibrium values.

Using

$$H_{II} = \frac{4\mu_0}{\sqrt{15}(Z+1)^{1/2}}\, l_2, \tag{12}$$

where $\mu_0 \simeq 0.96$ is a constant appearing in the ion viscosity $\mu_i = \mu_0 n_i k T_i \tau_i$,[31] the equations governing the plasma magnitudes inside the inner region II can be written, for any value of the ionization number Z, as[4,8]

$$\frac{\theta_i^{5/2}}{M_2}\frac{d\eta}{dy_i} = \eta - 1 + \frac{3}{5M_2^2}\left(\frac{Z}{Z+1}\frac{\theta_e}{\eta} + \frac{1}{Z+1}\frac{\theta_i}{\eta} - 1\right), \tag{13}$$

$$\frac{d\theta_e}{dy_i} = 0, \tag{14}$$

$$\frac{k_0}{2\mu_0 M_2}\theta_i^{5/2}\frac{d\theta_i}{dy_i} = \theta_i + \frac{5{M_2}^2(Z+1)}{9}\eta\,(\eta-2) + \frac{2}{3}\left(Z\theta_e \ln\eta - (Z+1)\,\eta\right) + G, \tag{15}$$

where $y_i = x/H_{II}$ and G is an integration constant that depends on the location of this inner region between the preheating and relaxation zones [these equations coincide with Eqs. (21)-(22) in Ref.[8]].

When using y as the spatial variable (i.e., in the external problem with length scale H_I), this inner region can be considered just as discontinuity for η and θ_i, where the jump is given by the Rankine-Hugoniot relations associated to (13)-(15). In

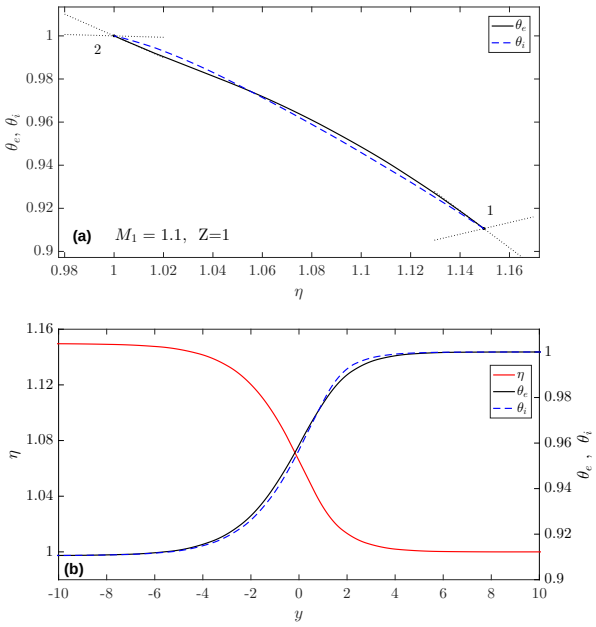

FIG. 1. Numerical solution of Eqs. (1)-(3) for $M_1 = 1.1$ and $Z = 1$.

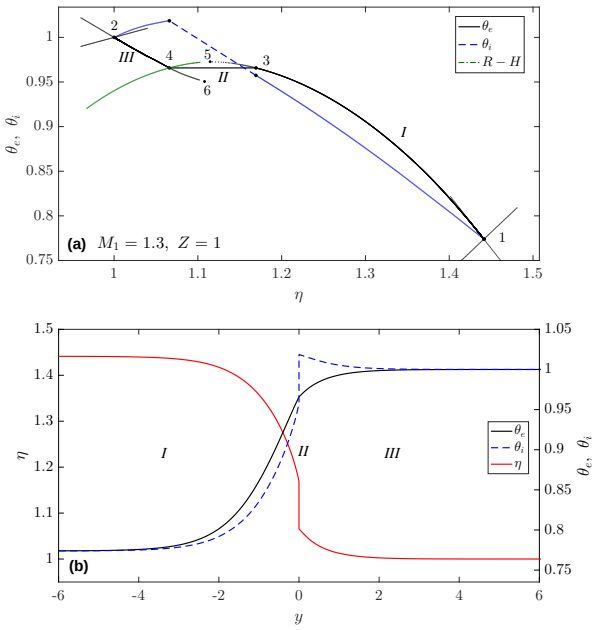

FIG. 2. Numerical solution of Eqs. (1)-(3) for $M_1 = 1.3$ and $Z = 1$. Also shown in (a) is the Rankine-Hugoniot $(R-H)$ relation in the phase space (16).

fact, considering that the internal shock lies between points labeled by 3 and 4, so that the plasma exhibits its changes through $1-3-4-2$ (see, for instance, Fig. 2 below for an example), and labelling the constant electron temperature across the ion shock as $\theta_{e3}(=\theta_{e4})$, the jump can be obtained by setting all derivatives in (13)-(15) to zero. Equation (13) becomes Eq. (1), that is used to eliminate the ion temperature

in Eq. (15), yielding constant G at the point 4, and the following algebraic relation between the plasma velocities η_3 and η_4 at the beginning and end of the inner shock, respectively:

$$5\left(\frac{5M_2^2}{3}+1\right)(\eta_3-\eta_4)-\frac{20M_2^2}{3}\left(\eta_3^2-\eta_4^2\right)= \frac{2Z}{Z+1}\theta_{e3}\ln\frac{\eta_3}{\eta_4}. \tag{16}$$

The corresponding θ_{i3} and θ_{i4} are given by Eq. (1) with $\theta_e=\theta_{e3}$, and $\eta=\eta_3$ and $\eta=\eta_4$, respectively.

Local linear analysis near the end singular points 1 and 2 of Eqs. (1)-(3) shows that these equations describe the evolution of the plasma throughout the shock, so that regions I and III merge and the inner shock II does not exist, if[3,8]

$$M_1<\sqrt{\frac{9Z+10}{5(Z+2)}}\equiv M^* \quad \text{or} \quad M_2>\sqrt{\frac{3Z+5}{5(Z+1)}}. \tag{17}$$

This critical Mach number varies monotonically from $M^*(Z=1)=\sqrt{19/15}\simeq 1.13$ to $M^*(Z\to\infty)=3/\sqrt{5}\simeq 1.34$ (see also Fig. 9 below).

In particular, if one writes Eqs. (1)-(3) as the autonomous system

$$\frac{d\theta_e}{d\eta}=\frac{f_2\{\theta_e,\eta\}}{f_3\{\theta_e,\eta\}}=f_{23}\{\theta_e,\eta\}, \tag{18}$$

once θ_i is eliminated from (1), it is shown that the upstream equilibrium point 1 is a saddle for any value of M_1, while the downstream equilibrium point 2 is a node for $1<M_1<M^*$, changing to a saddle point for $M^*<M_1<\infty$. For $M_1<M^*$ one has a weak or *relaxation shock*,[5] where a continuous solution to Eqs. (1)-(3) can be constructed numerically starting from the saddle point 1 and reaching the nodal point 2.

Figure 1 shows the results corresponding to $Z=1$ and $M_1=1.1$, which is smaller than $M^*(Z=1)\simeq 1.13$, plotted in the phase space, $\theta_e-\eta$ and $\theta_i-\eta$, and in terms of the physical coordinate y (we select $Z=1$ as the classical case for Hydrogen considered in most of the pioneering works on plasma shock waves). However, for stronger shocks ($M_1>M^*$), no such continuous solution exists, so that the discontinuity described above exists somewhere inside the *external* shock, separating regions I and III. In this case the numerical solution is much more complex to obtain than in the weak case, and consists of two numerical integrations of Eq. (18) starting from the equilibrium points 1 and 2 with the appropriate eigenvalues (remember that now both are saddle points), and joining them with the Rankine-Hugoniot conditions of the internal shock (16). This process is described in Fig. 2(a) in the phase space for $M_1=1.3$ and $Z=1$, where two numerical integrations of Eq. (18) are first made from point 1 to point 5, and from point 2 to point 6. Then, the Rankine-Hugoniot curve ($R-H$ in the figure) is used to obtain point 4 by its crossing with curve $2-6$, which yields also point 3 by tracing the line $\theta_e=\text{constant}=\theta_{e4}=\theta_{e3}$ towards the numerical solution $1-5$. The corresponding points for θ_{i3} and θ_{i4} are

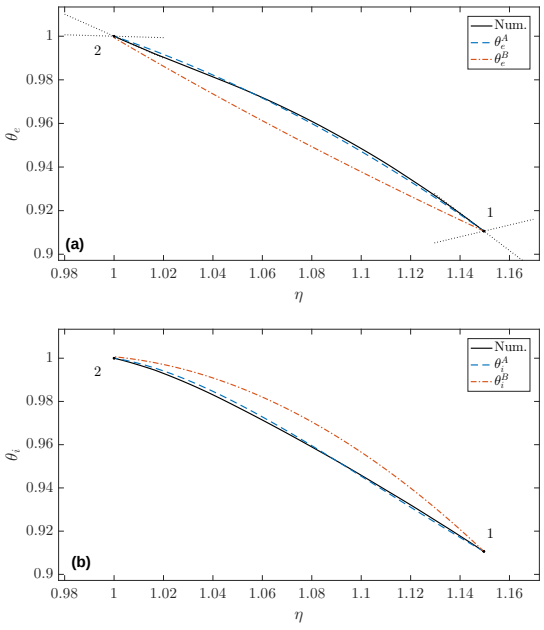

FIG. 3. Comparison between the approximations (19)-(20) and (21)-(23) (with $\alpha=1$) and numerical solutions from (1)-(3) for θ_e (a) and θ_i (b) when $M_1=1.1$ and $Z=1$.

obtained from the algebraic momentum equation (1). Once the solution is thus obtained in the phase space, the corresponding solution in the physical coordinate y is obtained by integrating Eqs. (1)-(3) for regions I and III, coupled with the internal shock by integrating Eqs. (13)-(15) from the saddle point 4 to the nodal point 3 of these equations[4,8] [see Fig. 2 (b)].

III. ANALYTICAL APPROXIMATE SOLUTIONS

A. Phase space solutions

Two approximate solutions are described here, first in the phase space, and then in terms of the spatial coordinate y.

The first one, denoted by the superscript 'A', is based on the fact that the electron and ion temperatures are very close to each other, not only near the upstream and downstream equilibrium states, but all through the shock for weak shocks (see Fig. 1) and in region I for stronger shocks. This feature was also noted in the pioneering works by Jukes[1] and Jaffrin and Probstein[4] for relaxation shocks with M_1 close to unity (and for $Z=1$), but these authors only developed the analytical approximate solution in the phase space for $\theta_e=\theta_i$, without obtaining the lowest order correction for θ_i in the phase space, nor the approximate solution in the physical space. Here we obtain the correction for θ_i for any Z, and extend the approximate solution to the physical coordinate y.

We first set $\theta_i=\theta_e$ in the momentum equation (1), to get

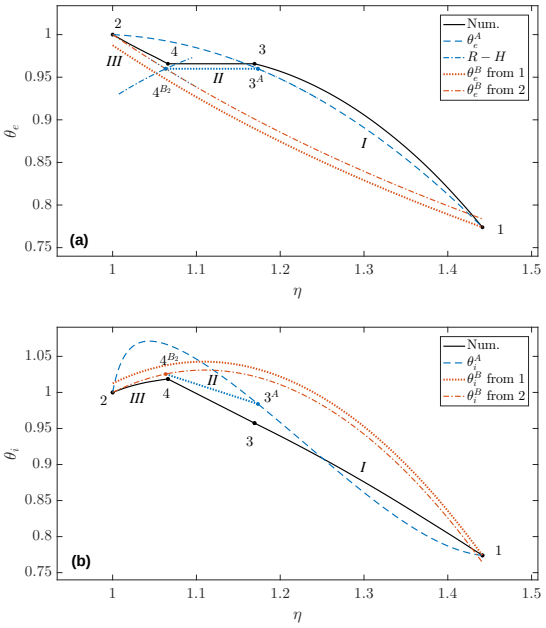

FIG. 4. Comparison between the approximations (19)-(20) and (21)-(23) (both with $\alpha = 1$ and 2) and numerical solutions from (1)-(3) for θ_e (a) and θ_i (b) when $M_1 = 1.3$ and $Z = 1$. Also included is the internal jump between point 3^A of $\theta_{e,i}^A$ and 4^{B_2} of $\theta_{e,i}^{B_2}$ from (16) and (1).

the following parabolic approximation for $\theta_e(\eta)$:

$$\theta_e^A = \left(\frac{5M_2^2}{3}+1\right)\eta - \frac{5M_2^2}{3}\eta^2. \tag{19}$$

Dividing (2) by (3), but without substituting θ_i from (1) like in (18), and using (19), one can obtain the following approximation for $\theta_i(\eta)$:

$$\theta_i^A = \theta_e^A - \\ -\eta\,\frac{125(\eta-1)M_2^2(Z+1)^2[(4\eta-1)M_2^2-3][(8\eta-5)M_2^2-3]}{36k_0Z^2[5(\eta-1)M_2^2-3][5(2\eta-1)M_2^2-3]}. \tag{20}$$

These expressions are compared with the numerical solutions in Figs. 3-4 for the same cases considered in Figs. 1-2. It is observed that the approximation works quite well all through the shock for weak or relaxation shocks ($M_1 < M^*$). However, for $M_1 > M^*$, when an internal ionic shock exists, it is only a reasonable approximation in the phase space in the preheating region I, being quite inaccurate in the relaxation region III downstream of the inner shock.

It is relevant to note that this approximation improves as Z increases, because (19) is an approximate solution of Eq. (1) for $Z \gg 1$ without assuming that $|\theta_i - \theta_e|$ is small. Thus, it is a convenient approximation even for not so weak relaxation shocks that contain an ion temperature overshoot when Z is sufficiently large, like the case depicted in Fig. 5 for $Z = 20$ (see also Fig. 7 below). Note that the approximation for $\theta_e^A(\eta)$ is almost indistinguishable from the exact numerical solution.

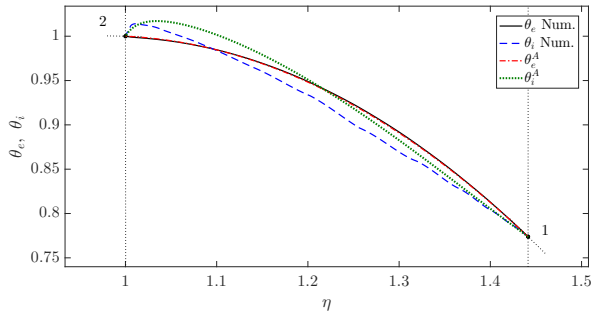

FIG. 5. Comparison between the approximations (19)-(20) and numerical solutions from (1)-(3) for $M_1 = 1.3$ and $Z = 20$.

As the second approximate solution in the phase space described here (actually, two approximate solutions, labelled with the superscripts 'B_α', with $\alpha = 1$ or 2) we assume that, at the lowest order, the electrons behave almost isentropically,

$$\theta_e^{B\alpha} \simeq \frac{C_\alpha}{\eta^{2/3}}, \tag{21}$$

where constant C_α depends on the equilibrium point ($\alpha = 1$ or 2) where the boundary condition is applied; i.e, $\theta_e = \eta = 1$ for $\alpha = 2$, and $\theta_e = \theta_1$ and $\eta = \eta_1$ given by Eqs. (6)-(7) for $\alpha = 1$, resulting

$$C_2 = 1, \quad C_1 = \frac{2^{16/3}M_1^{10/3}}{(M_1^2+3)^{5/3}(5M_1^2-1)}. \tag{22}$$

This approximation is likely to be valid in the downstream relaxation region, even for moderately strong shocks, where the electron temperature remains almost constant, particularly for large Z, when θ_{e3} approaches its final equilibrium value of unity.[8] Substituting (21) into the momentum equation (1), one obtains the corresponding lowest order approximation for the ion temperature:

$$\theta_i^{B\alpha} = -\frac{C_\alpha Z}{\eta^{2/3}} - \frac{1}{3}\eta(Z+1)[5(\eta-1)M_2^2-3]. \tag{23}$$

Figures 3 and 4 also contain this approximation B, starting from the equilibrium upstream condition $\alpha = 1$ for relaxation shocks ($M_1 < M^*$, Fig. 3), and from both equilibrium points, $\alpha = 1$ and 2, when an internal shock exists (Fig. 4). Clearly, the approximation B_1 is worse than A for relaxation shocks (Fig. 3), and in the preheating region I for strong shocks with internal ionic shock (Fig. 4), because electron heat conduction is obviously not negligible in these regions. But the approximation B_2 is much better than A along the ionic relaxation region III when $M_1 > M^*$ (Fig. 4). Thus, for strong shocks with an internal ionic shock, a reasonable algebraic approximation consists of solution A in the preheating region I and solution B_2 in the relaxation region III, both connected through the Rankine-Hugoniot relation (16), just like the numerical solution, but now all the solutions are algebraic in the three regions. Figure 4 shows both internal shocks, the exact

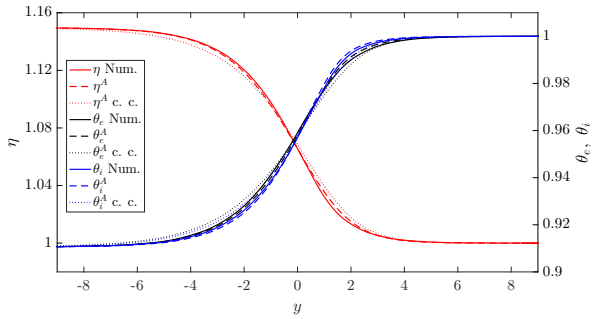

FIG. 6. Comparison between the numerical solution from (1)-(3) and the approximate solution A (19)-(20) in the physical coordinate y using (28) and the constant electron conductivity approximation (29) (labelled with c.c). $M_1 = 1.1$ and $Z = 1$.

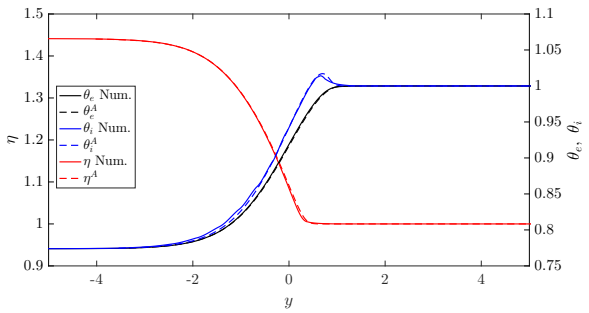

FIG. 7. Comparison between the numerical solution from (1)-(3) and the approximate solution A (19)-(20) in the physical coordinate y using (28) for $M_1 = 1.3$ and $Z = 20$.

numerical one and the approximation between point 4^{B_2}, intersection of the Rankine-Hugoniot relation of the inner shock with the approximate solution $\theta_{e,i}^{B_2}$, and point 3^A on the curves $\theta_{e,i}^A$, with $\theta_{e3}^A = \theta_{e4}^{B_2}$.

B. Complete solutions

To obtain the corresponding approximate solutions in the physical coordinate y we just need to compute the nondimensional velocity η as a function of y from the total energy equation (2), which can written as

$$\frac{d\theta_e}{d\eta}\frac{d\eta}{dy} = f_2\{\theta_e, \eta\}. \tag{24}$$

Since we know $\theta_e \simeq \theta_e^j(\eta)$ for any of the approximations j described above, this equation can formally be integrated to yield

$$y = A + \int \frac{d\theta_e^j(\eta)/d\eta}{f_2\{\theta_e^j(\eta), \eta\}} d\eta, \tag{25}$$

where A is an integration constant which allows us to 'center' the shock by locating the inflection point of $\eta(y)$ at $y = 0$ (say). This integration provides $\eta^j(y)$, through which $\theta_e^j(y)$ and $\theta_i^j(y)$ are given for any approximation $\theta_e^j(\eta)$.

For the approximation A [Eq. (19)], which in terms of η_1 is given by

$$\theta_e^A = \left(\frac{5}{4\eta_1 - 1} + 1\right)\eta - \frac{5}{4\eta_1 - 1}\eta^2 \tag{26}$$

one can write

$$y = A + \int d\eta \frac{(5\eta - 2 - 2\eta_1)(4 + 4\eta_1 - 5\eta)^{5/2}\eta^{5/2}}{6\sqrt{3}(1 - 4\eta_1)^2(\eta - 1)(\eta - \eta_1)}, \tag{27}$$

which yields

$$\begin{aligned} y = A &+ \sum_{i=1}^{5} a_i \eta^{i-1/2}\sqrt{4 + 4\eta_1 - 5\eta} \\ &+ a_6 \tan^{-1}\left\{\sqrt{\frac{5\eta}{4 + 4\eta_1 - 5\eta}}\right\} \\ &+ a_7 \tan^{-1}\left\{\frac{4 + 4\eta_1 + 5\sqrt{\eta}}{\sqrt{1 - 4\eta_1}(4 + 4\eta_1 - 5\eta)}\right\} \\ &+ a_8 \tan^{-1}\left\{\frac{5\sqrt{\eta} - 4 - 4\eta_1}{\sqrt{1 - 4\eta_1}(4 + 4\eta_1 - 5\eta)}\right\} \\ &+ a_9 \tanh^{-1}\left\{\sqrt{\frac{(\eta_1 - 4)\eta}{\eta_1(4 + 4\eta_1 - 5\eta)}}\right\}, \end{aligned} \tag{28}$$

where the coefficients a_i are given in the Appendix. As it is seen in Figs. 6-7, the combined solution (19), (20) and (28) provides a quite good approximation throughout the shock for relaxation shocks ($M < M^*$). Particularly for large Z (Fig. 7), when, as commented on above, the approximation A remains valid even if $|\theta_i - \theta_e|$ is not small. Figure 7 shows that the approximate solution captures quite well the overshot in the ion temperature, and yields a velocity and an electron temperature almost indistinguishable from the exact numerical solution.

It is worth noticing that the solution (28) is greatly simplified when one assumes a constant electron thermal conductivity, instead of Spitzer's thermal conductivity proportional to $\theta_e^{5/2}$, in the energy equation (2), yielding

$$y = A + \frac{\sqrt{4\eta_1 - 1}}{6\sqrt{3}} \ln\left[(\eta - 1)^{\frac{3-2\eta_1}{1-\eta_1}}(\eta - \eta_1)^{\frac{2-3\eta_1}{1-\eta_1}}\right]. \tag{29}$$

This approximate solution is formally similar to that previously found for the shock wave in a neutral gas with constant thermal conductivity in the limit of small Prandtl number,[27,28,30] but obviously with different constants and power coefficients in the present ionized gas problem with two temperatures, so that it yields, in addition to the corresponding velocity profile $\eta(y)$, two different temperature profiles for the electrons and for the ions. The corresponding solutions are also plotted in Fig. 6, showing a reasonable agreement with

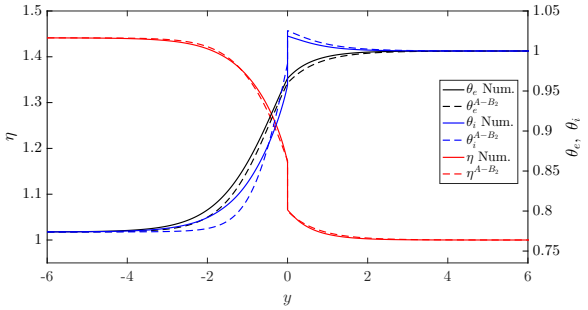

FIG. 8. Comparison in the physical coordinate y of the numerical solution from (1)-(3) with the approximate solution A in region I [(19)-(20) and (28)], and the approximate solution B_2 in region III [(21)-(23) and (31)], connected through the Rankine-Hugoniot relations [(16) and (1)] for the inner shock. $M_1 = 1.3$ and $Z = 1$.

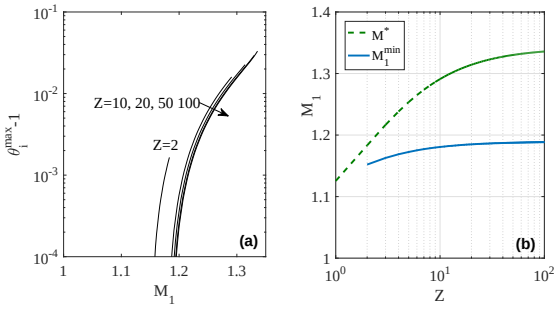

FIG. 9. Overshoot of the ion temperature from approximation A for a relaxation shock (a), appearing for $M_1^{min}(Z) \le M_1 \le M^*(Z)$, with M_1^{min} and M^* given in (b).

the exact numerical solution for this quite weak shock where the temperature variation across the shock is relatively small, and therefore the electron thermal conductivity is almost constant.

For stronger shocks ($M_1 > M^*$), the approximate solution B_2 for the region III is also needed in the physical coordinate y. Using (21), Eq. (25) can be written as

$$y = A + \int d\eta \frac{(4\eta_1 - 1)^{3/2}}{18\sqrt{3}(\eta - 1)(\eta - \eta_1)\eta^{10/3}}, \qquad (30)$$

which can be integrated to yield

$$\begin{aligned} y = &\sum_{i=1}^{3} b_i \eta^{i-2/3} + b_4 \tan^{-1}\left\{\frac{1+2\eta^{1/3}}{\sqrt{3}}\right\} \\ &+ b_5 \tan^{-1}\left\{\frac{\eta_1^{1/3} + 2\eta^{1/3}}{\sqrt{3}\eta_1^{1/3}}\right\} + b_6 \ln\left\{1 - \eta^{1/3}\right\} \\ &+ b_7 \ln\left\{1 + \eta^{1/3} + \eta^{2/3}\right\} + b_8 \ln\left\{\eta_1^{1/3} - \eta^{1/3}\right\} \\ &+ b_9 \ln\left\{\eta_1^{2/3} + (\eta_1\eta)^{1/3} + \eta^{2/3}\right\}, \end{aligned} \qquad (31)$$

where the coefficients b_i are given in the Appendix. Figure 8 shows that this global approximate solution, consisting of A in the preheating region I and B_2 in the relaxation region III connected through the Rankine-Hugoniot relations for the inner ionic shock II, is also a quite good approximation in the physical coordinate y throughout the shock when using (28) and (31) in their respective regions.

C. Ion temperature overshoot and shock wave thickness

One of the advantages of having approximate solutions is to be able to obtain easily, without costly computations, some relevant properties of the shock wave, though approximately.

For instance, the ion temperature overshoot in relaxation shocks (e.g., Fig. 7) can be obtained easily by computing the maximum of the algebraic expression (20). In doing so, one obtains that θ_i^{max} grows very fast with M_1 for constant Z, but decreases with Z for constant M_1 (see Fig. 9). Also, that no overshoot exists for $Z = 1$, within this approximation A for a relaxation shock, and that for $Z \ge 2$ it only exists above a threshold Mach number $M_1^{min}(Z)$, also plotted in Fig. 9 together with M^*. $M_1^{min} \simeq 1.152$ for $Z = 2$ and grows towards 1.190 as $Z \to \infty$.

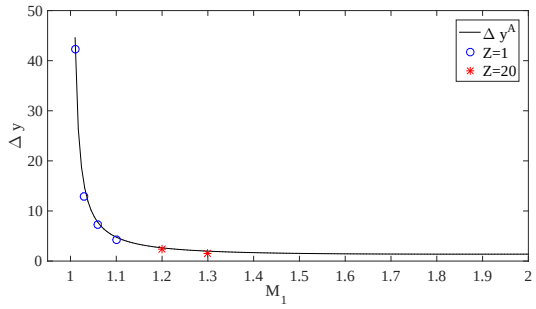

FIG. 10. Comparison between the shock wave thickness given by the approximation (33) (continuous line) with numerical results obtained for different values of Z and M_1 (symbols).

Another magnitude of interest is the shock wave thickness, particularly for relaxation shocks, since it may grow dramatically for very weak shocks ($M_1 \to 1$). Although the thickness can be defined in terms of different flow magnitudes, an appropriate form for relaxation shocks in terms of the plasma velocity is

$$\Delta y = \frac{\eta_1 - \eta_2}{\left|\frac{d\eta}{dy}\right|_{y=0}}, \qquad (32)$$

where $y = 0$ corresponds to the inflection point. Note from Eq. (24) that $(d\eta/dy)_{y=0}$ is the inverse of the integrand in Eq. (25) at $y = 0$. Using the approximation A given by Eq. (27), but evaluating $d\eta/dy$ at the middle point where $\eta = (\eta_1 + \eta_2)/2$, which approximately coincides with the inflection point for a relaxation shock, one obtains the following simple expression

for Δy, which is independent of the ionization number Z:

$$\Delta y^A = \frac{3(1+\eta_1)^6}{32(1-4\eta_1)^2(\eta_1-1)} = \\ = \frac{(5M_1^2+3)^6}{96(5M_1^2-1)^2(M_1^2+3)^3(M_1^2-1)}. \tag{33}$$

Figure 10 compares this expression as a function of M_1 with several thicknesses obtained directly from (32) using numerical solutions for $Z = 1$ and $Z = 20$ and different values of M_1. An excellent agreement is observed, corroborating that the thickness is actually almost independent of Z for relaxation shocks, as predicted by (33).

IV. CONCLUDING REMARKS

The algebraic approximate solutions given here are particularly simple in the phase space, both for fully relaxation shocks when $M_1 < M^*(Z)$, and for stronger shocks waves containing an inner ionic shock, where two algebraic solutions in the preheating and relaxation regions are connected through Rankine-Hugoniot relations for the internal shock. Of particular interest are relaxation shocks for large ionization number Z, where M^* can be sufficiently large for the relaxation shock to contain an important ion temperature overshoot inside, which is quite well predicted by the simple algebraic equations. Solutions in the physical spatial coordinate given here are algebraically more involved, but they agree quite well with exact numerical simulations for weak, and even for moderately strong, shocks. Alternatively, the algebraic solutions in the physical space are much simpler when the electron conductivity is assumed to be constant, but then the algebraic solution in the physical space is only approximately valid for very weak shock waves.

Appendix A: Coefficients of Eqs. (28) and (31)

$$a_1 = -\frac{(4\eta_1-1)^{3/2}\left(\eta_1^2+\eta_1+1\right)}{6\sqrt{3}\eta_1^3}, \tag{A1}$$

$$a_2 = \frac{\sqrt{5}\left(3\eta_1^3+34\eta_1^2+34\eta_1+3\right)}{18\sqrt{3}(1-4\eta_1)^2}, \tag{A2}$$

$$a_3 = \frac{\sqrt{5}\left(81\eta_1^2-88\eta_1+81\right)}{36\sqrt{3}(1-4\eta_1)^2}, \tag{A3}$$

$$a_4 = -\frac{15\sqrt{15}(\eta_1+1)}{8(1-4\eta_1)^2}, \tag{A4}$$

$$a_5 = \frac{25\sqrt{5}}{6\sqrt{3}(1-4\eta_1)^2}, \tag{A5}$$

$$a_6 = -\frac{33\eta_1^5-335\eta_1^4+705\eta_1^3+705\eta_1^2-335\eta_1+33}{15\sqrt{15}(1-4\eta_1)^2}, \tag{A6}$$

$$a_7 = \frac{\sqrt{1-4\eta_1}(2\eta_1-3)}{6\sqrt{3}(\eta_1-1)}, \tag{A7}$$

$$a_8 = \frac{\sqrt{1-4\eta_1}(2\eta_1-3)}{6\sqrt{3}(\eta_1-1)}, \tag{A8}$$

$$a_9 = -\frac{(-(\eta_1-4)\eta_1)^{5/2}(3\eta_1-2)}{3\sqrt{3}(1-4\eta_1)^2(\eta_1-1)}. \tag{A9}$$

$$b_1 = -\frac{(4\eta_1-1)^{3/2}\left(\eta_1^2+\eta_1+1\right)}{6\sqrt{3}\eta_1^3} \tag{A10}$$

$$b_2 = -\frac{(\eta_1+1)(4\eta_1-1)^{3/2}}{24\sqrt{3}\eta_1^2} \tag{A11}$$

$$b_3 = -\frac{(4\eta_1-1)^{3/2}}{42\sqrt{3}\eta_1} \tag{A12}$$

$$b_4 = -\frac{(4\eta_1-1)^{3/2}}{18(\eta_1-1)} \tag{A13}$$

$$b_5 = \frac{(4\eta_1-1)^{3/2}}{18(\eta_1-1)\eta_1^{10/3}} \tag{A14}$$

$$b_6 = -\frac{(4\eta_1-1)^{3/2}}{18\sqrt{3}(\eta_1-1)} \tag{A15}$$

$$b_7 = \frac{(4\eta_1-1)^{3/2}}{36\sqrt{3}(\eta_1-1)} \tag{A16}$$

$$b_8 = \frac{(4\eta_1-1)^{3/2}}{18\sqrt{3}(\eta_1-1)\eta_1^{10/3}} \tag{A17}$$

$$b_9 = -\frac{(4\eta_1-1)^{3/2}}{36\sqrt{3}(\eta_1-1)\eta_1^{10/3}} \tag{A18}$$

[1] J. D Jukes. The structure of a shock wave in a fully ionized gas. *J. Fluid Mech.*, 3:275–285, 1957.

[2] V. D. Shafranov. The structure of shock waves in a plasma. *Sov. Phys. JETP*, 5:1183–1188, 1957.

[3] V.S. Imshennik. Shock wave structure in a dense high-temperature plasma. *Sov. Phys. JETP*, 21:167–174, 1962.

[4]M. Y. Jaffrin and R. F. Probstein. Structure of a plasma shock wave. *Phys. Fluids*, 7:1658–1674, 1964.
[5]Ya. B. Zel'dovich and Yu. P. Raizer. *Physics of shock waves and high-temperature hydrodynamic phenomena*. Dover, New York, 2002.
[6]M. A. Liberman and A. L. Velikovich. *Physics of shock waves in gases and plasmas*. Springer, Berlin, 1986.
[7]T. O. Masser, J. G. Wohlbier, and R. B. Lowrie. Shock wave structure for a fully ionized plasma. *Shock Waves*, 21:367–381, 2011.
[8]J. Ramirez, J. R. Sanmartin, and R. Fernandez-Feria. Nonlocal electron heat relaxation in a plasma shock at arbitrary ionization number. *Phys. Fluids B: Plasma Physics*, 5:1485–1490, 1993.
[9]H. Yemin and H. Xiwei. The properties and structure of a plasma non-neutral shock. *Phys. Plasmas*, 10:2704–2711, 2003.
[10]R. B. Lowrie and J. D. Edwards. Radiative shock solutions with grey nonequilibrium diffusion. *Shock waves*, 18:129–143, 2008.
[11]B. M. Johnson and R. I. Klein. Three temperature plasma shock solutions with gray radiation diffusion. *Shock Waves*, 27:281–289, 2017).
[12]S. Eliezer and J. M. Martinez Val. The comeback of shock waves in inertial fusion energy. *Laser Part. Beams*, 29:175–181, 2011.
[13]B. Srinivasan, G. Kagan, and C. S. Adams. Multi-fluid studies of plasma shocks relevant to inertial confinement fusion. *J. Phys.: Conf. Series*, 717: 012054, 2016.
[14]S. Atzeni, X. Ribeyre, G. Schurtz, A. J. Schmitt, B. Canaud, R. Betti, and L. J. Perkins. Shock ignition of thermonuclear fuel: principles and modelling. *Nucl. Fusion*, 54:054008, 2014.
[15]R. S. Craxton, K. S. Anderson, T. R. Boehly, V. N. Goncharov, D. R. Harding, J. P. Knauer, R. L. McCrory, P. W. McKenty, D. D. Meyerhofer, and J. F. Myatt et al. Direct-drive inertial confinement fusion: A review. *Phys. Plasmas*, 22:110501, 2015.
[16]D. Kaganovich, M. H. Helle, D. F. Gordon, and A. Ting. Measurements and simulations of shock wave generated plasma-vacuum interface. *Phys. Plasmas*, 18:120701, 2011.
[17]R. M. Kulsrud. Important plasma problems in astrophysics. *Phys. Plasmas*, 2:1735–1745, 1995.
[18]S. Bouquet, R. Teyssier, and J. P. Chieze. Analytical study and structure of a stationary radiative shock. *Astrophys. J.*, 127:245–252, 2000.
[19]R. B. Lowrie and R. M. Rauenzahn. Radiative shock solutions in the equilibrium diffusion limit. *Shock waves*, 16:445–453, 2007.
[20]S. P. Kuo and S. S. Kuo. A physical mechanism of nonthermal plasma effect on shock wave. *Phys. Plasmas*, 12:012315, 2005.
[21]A. Markhotok, S. Popovic, and L. Vuskovic. The boundary effects of the shock wave dispersion in discharges. *Phys. Plasmas*, 15:032103, 2008.
[22]Q. Zhou, Z. Dong, and W. Yang. Revisiting the thermal effect on shock wave propagation in weakly ionized plasmas. *Phys. Plasmas*, 23:073508, 2016.
[23]I. V. Adamovich, I. Choi, N. Jiang, J.-H. Kim, S. Keshav, W. R. Lempert, E. Mintusov, M. Nishihara, M. Samimy, and M. Uddi. Plasma assisted ignition and high-speed flow control: non-thermal and thermal effects. *Plasma Sources Sci. Technol.*, 18:034018, 2009.
[24]Y. Ju and W. Sun. Plasma assisted combustion: Dynamics and chemistry. *Prog. Energy Comb. Sci.*, 48:21–83, 2015.
[25]R. Becker. Stosswelle und Detonation. *Z. Phys.*, 8:321–362, 1922.
[26]M. Morduchow and P. A. Libby. On a complete solution of the one-dimensional flow equations of a viscous, heat conducting, compressible gas. *J. Aeronaut. Sci.*, 16:674–684, 1949.
[27]B. M. Johnson. Closed-form shock solutions. *J. Fluid Mech.*, 745:R1–1–11, 2014.
[28]B. M. Johnson. Analytical shock solutions at large and small Prandtl number. *J. Fluid Mech.*, 726:R4–1–12, 2013.
[29]R. Fernandez-Feria and J. Fernandez de la Mora. Shock wave structure in gas mixtures with large mass disparity. *J. Fluid Mech.*, 179:21–40, 1987.
[30]R. Fernandez-Feria. Heavy gas relaxation in a light gas shock wave at small Prandtl number. *Phys. Rev. E*, 94:033108, 2016.
[31]S. I. Braginskii. Transport porcesses in a plasma. In M. A. Leontovich, editor, *Review of Plasma Physics*, volume 1, pages 205–311. Consultants Bureau, New York, 1965.
[32]L. Spitzer. *Physics of fully ionized gases*. Wiley, New York, 1962.